



UNIVERSITY OF LEEDS

This is a repository copy of *Kinetic Modeling for a Novel Permeable Reactive Biobarrier for In Situ Remediation of PAH-Contaminated Groundwater*.

White Rose Research Online URL for this paper:

<https://eprints.whiterose.ac.uk/183126/>

Version: Accepted Version

---

**Article:**

Liu, C, Yue, M, Banwart, SA et al. (4 more authors) (2022) Kinetic Modeling for a Novel Permeable Reactive Biobarrier for In Situ Remediation of PAH-Contaminated Groundwater. *Journal of Geotechnical and Geoenvironmental Engineering*, 148 (5). ISSN 0733-9410

[https://doi.org/10.1061/\(ASCE\)GT.1943-5606.0002779](https://doi.org/10.1061/(ASCE)GT.1943-5606.0002779)

---

© 2022 American Society of Civil Engineers. This is an author produced version of an article published in *Journal of Geotechnical and Geoenvironmental Engineering*. Uploaded in accordance with the publisher's self-archiving policy.

**Reuse**

Items deposited in White Rose Research Online are protected by copyright, with all rights reserved unless indicated otherwise. They may be downloaded and/or printed for private study, or other acts as permitted by national copyright laws. The publisher or other rights holders may allow further reproduction and re-use of the full text version. This is indicated by the licence information on the White Rose Research Online record for the item.

**Takedown**

If you consider content in White Rose Research Online to be in breach of UK law, please notify us by emailing [eprints@whiterose.ac.uk](mailto:eprints@whiterose.ac.uk) including the URL of the record and the reason for the withdrawal request.



[eprints@whiterose.ac.uk](mailto:eprints@whiterose.ac.uk)  
<https://eprints.whiterose.ac.uk/>

1 **Kinetic modelling for a novel permeable reactive bio-barrier for in-situ**  
2 **remediation of PAH-contaminated groundwater**

3 Cuicui Liu<sup>a,b</sup>, Yue Ma<sup>c</sup>, Steven A. Banwart<sup>d,e</sup>, Xiaohui Chen<sup>f,\*</sup>, Wenchao Du<sup>g</sup>, Ying  
4 Yin<sup>h</sup>, Hongyan Guo<sup>i,\*</sup>

5  
6 <sup>a</sup>State Key Laboratory of Pollution Control and Resource Reuse, School of the  
7 Environment, Nanjing University, Nanjing, 210023, China

8 <sup>b</sup>School of Civil Engineering, University of Leeds, Leeds, LS2 9JT, UK

9 <sup>c</sup>School of Civil Engineering, University of Leeds, Leeds, LS2 9JT, UK

10 <sup>d</sup>School of Earth and Environment, University of Leeds, Leeds, LS2 9JT, UK

11 <sup>e</sup>Global Food and Environment Institute, University of Leeds, Leeds, LS2 9JT, UK

12 <sup>f</sup>School of Civil Engineering, University of Leeds, Leeds, LS2 9JT, UK

13 <sup>g</sup>School of the Environment, Nanjing Normal University, Nanjing, 210023, China

14 <sup>h</sup>State Key Laboratory of Pollution Control and Resource Reuse, School of the  
15 Environment, Nanjing University, Nanjing, 210023, China

16 <sup>i</sup>State Key Laboratory of Pollution Control and Resource Reuse, School of the  
17 Environment, Nanjing University, Nanjing, 210023, China

18 \*Correspondence: Xiaohui Chen and Hongyan Guo, tel.: +44(0)113 343 0350

19 E-mail: [x.chen@leeds.ac.uk](mailto:x.chen@leeds.ac.uk) and [hyguo@nju.edu.cn](mailto:hyguo@nju.edu.cn)

20

21 **Abstract**

22 Permeable reactive barriers (PRBs) are an environmentally-friendly and cost-effective  
23 *in situ* remediation technology and have been used to restore polycyclic aromatic  
24 hydrocarbons (PAHs)-contaminated groundwater. However, the understanding of  
25 removal mechanisms of the pollutant from groundwater remains as a challenge due to  
26 the complex interactions between microbial evolution, organic carbon kinetics and  
27 multiple chemical reactions. In this study, a one-dimensional reactive transport model  
28 was developed to study 450-day column experiments for removal of phenanthrene  
29 from groundwater using new PRB materials A (including wheat straw) and B  
30 (including coconut shell biochar). The modelling results provided a deeper  
31 understanding of the removal process for phenanthrene that material B had a higher  
32 removal efficiency than A over 34 days. The removal efficiency of phenanthrene in  
33 both A and B was close to 100% in the PRB system. This is because: (1) Material B  
34 had a higher adsorption capacity for phenanthrene than material A. Adsorption played  
35 an important role in the short term (e.g. 20 days), whereas, biodegradation controlled  
36 longer-term removal processes. (2) The biomass in column B was higher ( $p < 0.05$ )  
37 than in column A. (3) B had a higher microbial yield coefficient that could favor  
38 longer-term microbial growth and biodegradation activity. Material B might have a  
39 greater potential than A for longer-term remediation performance. The simulated  
40 results were generally in agreement with the experimental results and supported the  
41 development of field-scale pilot testing of these materials for groundwater

42 remediation.

43

44 Keywords: Phenanthrene; PHREEQC; Kinetics; Permeable reactive barrier;

45 Groundwater remediation

46

## 47 **1. Introduction**

48 Polycyclic aromatic hydrocarbons (PAHs) are potentially mutagenic and carcinogenic  
49 to humans (Ferreira et al. 2013). The groundwater in Northern, Northeastern,  
50 Southeastern, and Southwestern China is severely polluted by PAHs. Research has  
51 reported that PAHs can be biodegraded to CO<sub>2</sub> and H<sub>2</sub>O by microbes under aerobic  
52 conditions and the biodegradation rate of PAHs can be influenced by dissolved  
53 oxygen (DO) levels (Haritash and Kaushik 2009; Waigi et al. 2015). The  
54 concentration of DO in groundwater is generally very low (< 3 mg/L) (Yeh et al.  
55 2010). Hence, the biodegradation of PAHs may be limited by the low concentration of  
56 DO and by the relatively low solubility of PAHs in the aqueous phase. Therefore, the  
57 main challenges for *in situ* bioremediation of PAHs contaminated groundwater are the  
58 choice of a suitable carbon substrate and the supply of reactive oxygen species.  
59 Calcium peroxide (CaO<sub>2</sub>) is an efficient oxygen-releasing compound, which could  
60 provide DO for the bioremediation of PAH-contaminated groundwater (Lin et al.  
61 2017). Biochar is an economical and readily available carbonaceous porous material  
62 (Mohanty et al. 2018). Straw has already been utilized as a low-cost carbon source  
63 material for groundwater remediation (Zhang et al. 2017). Therefore, calcium  
64 peroxide and straw/biochar have potential to be used in combination for permeable  
65 reactive barriers (PRBs), but they have infrequently been used in PAHs  
66 biodegradation applications so far.

67 PRBs have been a mature remediation technology for the treatment of polluted

68 groundwater for decades (Basu and Johnson 2012). The removal efficiency of the  
69 pollutant using PRBs depends on the type of reactive media used and the removal  
70 mechanism. Studies have shown that PRBs can successfully remove various  
71 pollutants transported by groundwater flow, including heavy metals, chlorinated  
72 solvents, aromatic hydrocarbons, and pesticides (Gandhi et al. 2002). However, PRBs  
73 have not been widely used to remove PAHs due to the limited available reactive  
74 media (Cobas et al. 2014). Phenanthrene is the smallest characteristic unit of  
75 carcinogenic PAHs (Wang et al. 2020) and is one of the most abundant PAHs in  
76 aquatic ecosystems. The ubiquitous distribution of phenanthrene in the aquatic  
77 environment and its tendency for accumulation within organisms results in the  
78 potential for deleterious effects (Hannam et al. 2010). In our previous research, we  
79 developed novel PRB materials that relied on a microbial self-domestication  
80 mechanism to remediate phenanthrene-contaminated groundwater (Liu et al. 2019).  
81 Column experiments were conducted to investigate the suitability of novel PRB  
82 materials for remediation of PAH-contaminated groundwater, including the adsorption  
83 and biodegradation of phenanthrene, the duration of carbon and reactive oxygen  
84 release, and the change in the relative abundance of active microbial biomass.

85 The aim of the current work is to simulate the results of column experiments with  
86 the geochemical modelling code PHREEQC as a quantitative analysis framework to  
87 gain a deeper understanding of the removal process of phenanthrene from  
88 groundwater using PRB technology. The combined mechanism of adsorption and

89 biodegradation were responsible for phenanthrene removal in columns A and B. We  
90 assumed that materials A and B firstly adsorbed phenanthrene from groundwater.  
91 Then, phenanthrene was degraded by microorganisms with the increase of biomass in  
92 columns A and B. The previous research has showed the potential of microorganisms  
93 aerobically degrading phenanthrene, with DO as the terminal electron acceptor  
94 (Moscoso et al. 2012). The calcium peroxide component of materials A and B could  
95 efficiently provide oxygen for aerobic biodegradation of phenanthrene and the  
96 oxidation of dissolved total organic carbon (TOC). The organic carbon was released  
97 from straw or biochar, which may maintain the capacity of microbes to degrade  
98 phenanthrene when the concentrations of phenanthrene were low. The dissolved  
99 organic carbon in columns A and B was assumed to be the carbon and energy source  
100 to support microbial growth.

101

## 102 **2. Material and methods**

### 103 **2.1. Experimental study**

104 A new PRB material was developed for the remediation of phenanthrene  
105 contaminated groundwater. The PRB materials A and B were both pellets that had a  
106 three-layer structure including a wood brick core, a packed layer, and an outer shell.  
107 Materials A and B had the same reactive oxygen source (calcium peroxide), but with  
108 different carbon source (wheat straw and coconut shell biochar). The diatomite,  
109 attapulgite, and Portland cement in the materials served as adhesive components. The

110 materials were bound by sodium alginate mixed with water. Detailed information  
111 about the composition of the PRB material is given in Table 1.

112 A 450-day column experiment was conducted to assess the capacity of the new  
113 PRB materials to remove phenanthrene from groundwater. The length of glass  
114 columns was 50 cm and the inner diameter was 4 cm. Columns A and B were  
115 equipped with four sampling ports (named SP1-4) spaced at 10 cm intervals. The  
116 columns were packed with a homogenous mixture of either material A or B and quartz  
117 sand (1:1, v/v). The materials A and B in the columns were bounded by a 5 cm-layer  
118 sand at both the bottom and the top. The relatively high concentrations of  
119 phenanthrene in groundwater ranged from 0.2 to 1 mg/L (Broholm et al. 1999;  
120 Ebihara and Bishop 2002; Zhang et al. 2019). The flow rate was chosen to simulate  
121 typical flow conditions of shallow aquifers, which corresponded to a flow velocity of  
122 less than 2 m day<sup>-1</sup> (Folch et al. 2013). The phenanthrene (0.9 mg/L) contaminated  
123 groundwater was pumped into the columns at a flow rate of 126.89  $\mu\text{L min}^{-1}$  by the  
124 peristaltic pump. The corresponding flow velocity transported in the columns was  
125 about 0.48 m day<sup>-1</sup>, which was less than 2 m day<sup>-1</sup> noted for shallow groundwater flow.  
126 A total of 53.02 L per year of groundwater flowed through the column. The details of  
127 the columns are shown in Table 2.

128 The effluent of the columns was frequently sampled. The pH and DO were  
129 measured immediately after collecting the samples from the columns using a portable  
130 analyzer (Orion 5 Star, Thermo, USA). The TOC concentrations were determined



131 using a total organic carbon analysis meter (TOC-Aurora 1030D, OI, US). The  
132 phenanthrene concentrations were determined using high performance liquid  
133 chromatography (HPLC 1200, Agilent, USA). The details for phenanthrene  
134 adsorption experiments of materials A and B were shown in Liu et al. (2019). After  
135 the column experiments had run for 200 days, samples of the materials were collected  
136 from the sampling ports in columns A and B. Subsamples (0.5 g) were taken from  
137 these samples and the DNA was extracted using a FastDNA<sup>TM</sup> SPIN Kit for soils. The  
138 V4 region of the bacterial 16S rRNA gene was amplified using the 515F  
139 (5'-GTGCCAGCMGCCGCGGTAA-3') and 806R  
140 (5'-GGACTACHVGGGTWTCTAAT-3') primers for pyrosequencing on a sequencer  
141 (MiSeq) (Caporaso et al. 2012; Caporaso et al. 2011).

142

## 143 **2.2. Column experiments analysis and kinetic results**

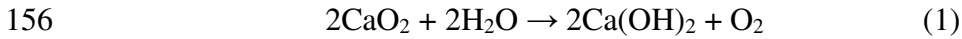
144 The modelling study considered the 450-day column experimental process, and  
145 focused on adsorption and microbial degradation processes for the removal of  
146 phenanthrene from groundwater. The kinetic information for the remediation of  
147 phenanthrene contaminated groundwater using the PRB system obtained from the  
148 literature is summarized below.

149

### 150 **2.2.1. pH and dissolved oxygen**

151 The materials A and B were assumed to gradually release calcium peroxide into the

152 flowing groundwater, which could cause the rise of pH value and the increase of  
153 dissolved molecular oxygen in the columns. The initial mass of CaO<sub>2</sub> in materials A  
154 and B were calculated as 0.330 and 0.315 mol, respectively. The reaction between  
155 CaO<sub>2</sub> and water can be described as follows:



157 The reaction equation of CaO<sub>2</sub> used in this paper is widely accepted in the literature  
158 and has been adopted by different authors investigating CaO<sub>2</sub> reaction both in  
159 experimental and modelling studies (Chen et al. 2012). The release rates of CaO<sub>2</sub> in A  
160 and B columns were assumed constant with value of  $7.17 \times 10^{-8}$  and  $6.88 \times 10^{-8}$  mol L<sup>-1</sup>  
161 s<sup>-1</sup>, respectively, so as to obtain the best fit of the model to the experimental data. The  
162 production rate of DO ( $R_{ox} = \lambda$ ) in A and B columns based on equation (1) should be  
163  $3.58 \times 10^{-8}$  and  $3.44 \times 10^{-8}$  mol L<sup>-1</sup> s<sup>-1</sup>, respectively.

164

### 165 **2.2.2. Phenanthrene adsorption in columns A and B**

166 The retardation of contaminants due to the process of adsorption can be modeled with  
167 a linear reversible sorption expression characterized by a constant distribution  
168 coefficient (defined below). The rate of phenanthrene adsorption is given by  
169 Tebes-Stevens et al. (1998):

$$170 \quad R_{phen,sorp} = -k_m \left( C_{phen,pw} - \frac{C_{phen,s}}{K_d} \right) \quad (2)$$

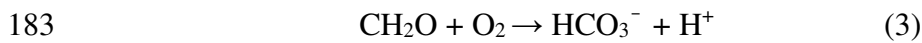
171 where  $R_{phen,sorp}$  is the adsorption rate (mol L<sup>-1</sup> s<sup>-1</sup>) of phenanthrene,  $C_{phen,pw}$   
172 denotes the aqueous concentration (mol L<sup>-1</sup>) of phenanthrene,  $C_{phen,s}$  denotes the

173 adsorbed concentration (mol g<sup>-1</sup>) of phenanthrene,  $k_m$  is the mass transfer coefficient  
174 (s<sup>-1</sup>), and  $K_d$  is the distribution coefficient (L g<sup>-1</sup>) for the linear equilibrium  
175 adsorption. The value of  $k_m$  and  $K_d$  were obtained in accordance with the  
176 column-type modelling processes used to describe dynamic adsorption mass transfer  
177 (Pantić et al. 2019; Tebes-Stevens et al. 1998).

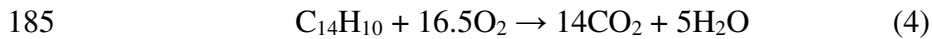
178

### 179 **2.2.3. Phenanthrene biodegradation and biomass increase in columns A and B**

180 The microbes could use organic carbon as a carbon and energy source, which is  
181 chemically defined in our modelling simulations as CH<sub>2</sub>O. The degradation of organic  
182 carbon can be described by the reaction:



184 The stoichiometric equation for the complete mineralization of phenanthrene is:



186 The gross growth of the biomass,  $\mu$  (s<sup>-1</sup>), is assumed to be limited by the availability  
187 of substrate and molecular oxygen, which is expressed with a multiple substrate  
188 Monod equation (Ai 2007; Berge et al. 2007; Geng et al. 2013; Wu et al. 2015):

$$189 \quad \mu = \mu_{max,s} \frac{C_{s,pw}}{K_s + C_{s,pw}} \frac{C_{ox,pw}}{K_{ox} + C_{ox,pw}} \quad (5)$$

190 where  $\mu_{max,s}$  is the maximum growth rate (s<sup>-1</sup>),  $C_{s,pw}$  is the aqueous concentration  
191 (mol L<sup>-1</sup>) of the substrate (phenanthrene or TOC) as electron donor,  $K_s$  is the  
192 half-maximum rate concentration (mol L<sup>-1</sup>) of the substrate,  $C_{ox,pw}$  is dissolved  
193 molecular oxygen concentration (mol L<sup>-1</sup>) as electron acceptor and  $K_{ox}$  is the

194 half-maximum rate concentration ( $\text{mol L}^{-1}$ ) of DO. The dissolved molecular oxygen  
 195 was mainly consumed by the degradation of phenanthrene and the oxidation of  
 196 dissolved total organic carbon in columns A and B. The Monod kinetic parameters  
 197 (e.g.  $\mu_{max,s}$ ,  $K_s$ , and  $K_{ox}$ ) were taken from the studies related to the degradation of  
 198 organic compounds (Carboneras et al. 2017; Krishnan et al. 2017; Lokshina et al.  
 199 2001; McClure and Sleep 1996; Tebes-Stevens et al. 1998; Verce et al. 2000), which  
 200 could obtain the best fit of the model to the measured results.

201 The substrate consumption was assumed to be a function of the biomass  
 202 concentration (Carvajal et al. 2018; Geng et al. 2013; Safdari et al. 2018):

$$203 \quad R_{s,bio} = \frac{ds}{dt} = -\frac{\mu}{Y_{X_s}} X_s \quad (6)$$

204 where  $R_{s,bio}$  is the rate ( $\text{mol L}^{-1} \text{s}^{-1}$ ) of substrate consumption,  $\mu$  is the gross growth  
 205 rate ( $\text{s}^{-1}$ ) of the biomass,  $X_s$  is the concentration ( $\text{mol biomass C L}^{-1}$ ) of biomass,  $Y_{X_s}$   
 206 is microbial yield coefficient ( $\text{mol biomass C/mol substrate C}$ ). The consumption rate  
 207 of phenanthrene and dissolved organic carbon can be defined as shown below,  
 208 respectively:

$$209 \quad R_{phen,bio} = -\frac{\mu_{max,phen} X_{phen}}{14Y_{X_{phen}}} \frac{C_{phen,pw}}{K_{phen} + C_{phen,pw}} \frac{C_{ox,pw}}{K_{ox} + C_{ox,pw}} \quad (7)$$

$$210 \quad R_{TOC,bio} = -\frac{\mu_{max,TOC} X_{TOC}}{Y_{X_{TOC}}} \frac{C_{TOC,pw}}{K_{TOC} + C_{TOC,pw}} \frac{C_{ox,pw}}{K_{ox} + C_{ox,pw}} \quad (8)$$

211 The carbon content of the biomass was estimated using the carbon content per  
 212 bacterial cell (i.e.  $9.4 \times 10^{-14} \text{ g C/cell}$ ) (Acharya et al. 2019). The rate of biomass  
 213 accumulate or loss is dependent on the rate of substrate utilization and a first-order  
 214 decay rate for the biomass (Akobi et al. 2017). Therefore, the change rate of biomass

215 concentration on phenanthrene and dissolved organic carbon are given by the  
216 equations, respectively (Balakrishnan et al. 2019):

$$217 \quad R_{bm,phen} = -14Y_{X_{phen}}R_{phen,bio} - bX_{phen} \quad (9)$$

$$218 \quad R_{bm,TOC} = -Y_{X_{TOC}}R_{TOC,bio} - bX_{TOC} \quad (10)$$

219 where  $R_{bm,phen}$  is the rate (mol biomass C L<sup>-1</sup> s<sup>-1</sup>) of biomass growth on  
220 phenanthrene,  $R_{bm,TOC}$  is the rate (mol biomass C L<sup>-1</sup> s<sup>-1</sup>) of biomass growth on TOC,  
221  $b$  is first-order microbial decay coefficient (s<sup>-1</sup>).

222 The yield coefficient  $Y_{X_s}$  links microbial growth to carbon consumption. It is  
223 defined as the ratio of organic carbon incorporated into cell mass in a given time  
224 interval to the total organic carbon consumption. The values of  $Y_{X_{phen}}$  for  
225 phenanthrene in columns A and B were selected as 0.44 and 0.53, respectively. The  
226  $Y_{X_{TOC}}$  for dissolved organic carbon in columns A and B were defined as 0.932 and  
227 0.954, respectively. The values of  $Y_{X_s}$  were adjusted based on inspection of the fit of  
228 simulation results to experimental data. The first-order biodecay is appropriate only  
229 when the substrate is the growth-limiting factor and the bacterial concentration is  
230 relatively high. The value of microbial decay rate was obtained based on Chen and  
231 McTernan (1992), who suggested the  $b$  value for bacteria.

232

### 233 **2.3. Modelling approach**

234 The PHREEQC Interactive Program (version 3.4.0.12927) is available from the U.S.  
235 Geological Survey, which is based on an ion-association equilibrium aqueous

236 speciation model and has capabilities for batch-reaction and one-dimensional (1-D)  
237 transport calculations (Boluda-Botella et al. 2014). With respect to the numerical  
238 method for transport modelling, PHREEQC can simulate several one-dimensional  
239 transport processes: diffusion, advection, and dispersion, as well as advection and  
240 dispersion with diffusion into stagnant zones. The wateq4f database of PHREEQC  
241 was used to calculate the chemical speciation of major elements in the study (Bartzas  
242 and Komnitsas 2010).

243 The conceptual model was established according to information from both  
244 theoretical and experimental analysis. Fig. 1 shows a schematic diagram of the  
245 column experiment processes and the major physiochemical and biological  
246 mechanisms involved. Adsorption and microbial degradation processes for  
247 phenanthrene were considered in the model. It was assumed that the consumption of  
248 dissolved organic carbon attributed to supporting the growth of microorganisms as  
249 carbon source. The calcium peroxide as oxygen source supported the biodegradation  
250 of phenanthrene and the oxidation of dissolved organic carbon. According to the  
251 conceptual model, the transport processes considered in the model were simulated  
252 using the advection-dispersion reaction (ADR) equation:

$$253 \quad \frac{\partial C_i}{\partial t} = -v \frac{\partial C_i}{\partial x} + D_L \frac{\partial^2 C_i}{\partial x^2} + \sum_{m=1}^n R_{im} \quad (11)$$

254 where:  $C$  is the concentration of species in water ( $\text{mol L}^{-1}$ ),  $i$  represents the different  
255 species,  $t$  is time (s),  $v$  is pore water flow velocity ( $\text{m s}^{-1}$ ),  $x$  is distance (m),  $D_L$   
256 is the hydrodynamic dispersion coefficient ( $\text{m}^2 \text{s}^{-1}$ ,  $D_L = D_e + \alpha_L v$ , with  $D_e$  the

257 diffusion coefficient, and  $\alpha_L$  the dispersivity (m)),  $n$  is the total number of reactions,  
 258 and  $R_{im}$  is the reaction rate ( $\text{mol L}^{-1} \text{ s}^{-1}$ ) or ( $\text{mol biomass C L}^{-1} \text{ s}^{-1}$ ). The term  $v \frac{\partial C_i}{\partial x}$   
 259 represents advective transport,  $D_L \frac{\partial^2 C_i}{\partial x^2}$  gives dispersive transport. The ADR equations  
 260 for the local change of species concentrations in porewater or solids are presented in  
 261 Table 3. The Cauchy boundary condition (Type 3 or flux) (Eq. (12)) was specified for  
 262 both inlet and outlet boundaries.

$$263 \quad C(x_{end}, t) = C_0 + \frac{D_L}{v} \frac{\partial C(x_{end}, t)}{\partial x} \quad (12)$$

264 where  $C$  is the concentration in water ( $\text{mol L}^{-1}$ ),  $t$  is time (s),  $v$  is the pore-water  
 265 flow velocity ( $\text{m s}^{-1}$ ),  $x$  is distance (m),  $D_L$  is the hydrodynamic dispersion  
 266 coefficient ( $\text{m}^2 \text{ s}^{-1}$ ). A flux was used as the groundwater flow boundary condition at  
 267 the start and end cells. There were no measured values for diffusion coefficients and  
 268 dispersivity in the experiment. A value of 0.5 cm was defined for dispersivity which  
 269 was in the common range of column scales (Kohfahl and Pekdeger 2006). The  
 270 diffusion coefficient was assumed to be  $0.03 \times 10^{-9} \text{ m}^2 \text{ s}^{-1}$  (Obiri-Nyarko et al. 2015).  
 271 The model transport parameters are showed in Table 4.

272 The transport of the pollutant solution in columns was divided computationally into  
 273 10 equal cells in series along the column, in which the solution advected with a fixed  
 274 residence time in each cell. The core blocks using in the PHREEQC code included  
 275 SOLUTION, PHASES, REACTION, RATES, KINETICS, and TRANSPORT. The  
 276 reaction and kinetics parameter values (Table 5) were obtained from either the  
 277 experiment or published literature, which were utilized to define the model. The

278 modelling results for the values of state variables pH, DO, TOC, and phenanthrene  
279 concentrations were collated from results for the final cell of the columns (cell 10),  
280 which was corresponding to the experimental results in the effluent of columns A and  
281 B. In the simulations, in order to further assess the removal capacity of the columns  
282 for phenanthrene. The phenanthrene concentration of the initial solution was set to 0.9,  
283 1.5, 2, and 2.5 mg/L, respectively. The simulated results for the biomass were collated  
284 from results for the cells 1, 4, 7, and 9, which were compared with the experimental  
285 results of the biomass from SP1-SP4 of columns A and B. The results of the model  
286 calculations were compared with the experimentally measured results. The findings  
287 from the numerical modelling and theoretical analysis were combined to provide a  
288 deeper quantitative understanding of phenanthrene removal processes from  
289 groundwater using PRB technology with these materials.

290

### 291 **3. Results and discussion**

#### 292 **3.1. Modelling of column experiments**

293 The processes of the conceptual model for the column experiments have been  
294 mathematically modelled using the mixed equilibrium reaction and kinetics approach  
295 with the PHREEQC code. Changes in pH value, DO, TOC, phenanthrene  
296 concentration, and biomass, as measured in the column experiment, have been  
297 analyzed as state variables in the modelling simulations.

298



### 299 **3.1.1. pH value and DO**

300 The modelling and experimental results for pH and DO in the effluent of columns A  
301 and B are displayed in Figs. 2a-b. The pH value and DO concentration of the initial  
302 solution was about 7.0 and 0.14 mmol/L, respectively. The experimental results  
303 showed that the pH in the effluent of columns A and B was between 9.82 and 10.94,  
304 likely because  $\text{Ca(OH)}_2$  formed from the  $\text{CaO}_2$ , and caused the pH to rise. The high  
305 pH may cause the inhibition of the microbial growth and biological enzyme activity  
306 (Zhang et al. 2018). The addition of the phosphate buffer may be able to neutralize the  
307 high pH (Lee and Fan 2020). The DO concentration in the effluent of columns A and  
308 B ranged from 0.19 to 0.32 mmol/L, which was higher than the initial solution. These  
309 data indicated that the  $\text{CaO}_2$  incorporated in materials A and B acted as a slow-release  
310 source of DO. Sponza and Gok (2011) reported that the DO concentrations for the  
311 treatment of phenanthrene contaminated wastewater were between 0.125 and 0.188  
312 mmol/L. Thus, the dissolved oxygen was enough for aerobic degradation of  
313 phenanthrene in the columns. The modelling results exhibited DO concentrations in  
314 columns A and B that rapidly increased to 0.28 and 0.29 mmol/L due to the chemical  
315 reaction between calcium peroxide and water causing the production of DO,  
316 respectively, on the 30th day. After that, the DO concentrations of columns A and B  
317 remained at about 0.28 and 0.29 mmol/L, respectively, because of the continuous  
318 release of calcium peroxide from materials. The pH value of columns A and B  
319 changed from 7.0 to 10.76 in the modelling results. Consequently, the modelling

320 results of pH and DO for columns A and B were in agreement with the experimental  
321 results.

322

### 323 **3.1.2. TOC**

324 Fig. 2c provides the information about the modelling and experimental data of TOC in  
325 the effluent of columns A and B. For the experimental results, the TOC concentration  
326 of column A increased significantly and reached 41.7 mmol/L in the beginning, but  
327 then dropped and was between 11.5 and 15.3 mmol/L in the remainder of the  
328 experiment. This was assumed to occur because the wheat straw decomposition was  
329 determined by the soluble fraction of the chemical components of straw during the  
330 early stages, and then, it was largely dependent on mineralization of the insoluble  
331 pool of straw (Cogle et al. 1989). However, the TOC concentration of column B  
332 remained relatively stable and ranged from 6 to 16.3 mmol/L. In the simulation, the  
333 initial TOC concentration in columns A and B was defined as 15.8 and 16.4 mmol/L,  
334 which was calculated according to the TOC concentration (12.94 mmol/L) of the  
335 initial solution and the organic carbon released from the materials A (1.79 g C) and B  
336 (2.17 g C) each year. The modelling results showed that the TOC concentrations of  
337 columns A and B increased to 15.12 and 15.51 mmol/L on the 34th day, respectively.  
338 Then, the TOC concentrations of columns A and B began to decrease due to the  
339 consumption as a carbon and energy source supporting the microbial growth. Based  
340 on these results, we concluded that the TOC concentrations from the modelling results

341 were primarily consistent with the experimental results. However, the trend in the  
342 release of organic carbon from columns A and B could not be accurately simulated. It  
343 was difficult to parameterise relevant rate equations for the release process of organic  
344 carbon from columns A and B, so we simulated the consumption of organic carbon to  
345 represent the change of organic carbon in columns A and B.

346

### 347 **3.1.3. The change of phenanthrene concentration**

348 The modelling and experimental results of phenanthrene concentration in the effluent  
349 of columns A and B are depicted in Fig. 2d. The concentration of phenanthrene in the  
350 effluent of columns A and B was not detected during the entire experiment. The  
351 modelling results showed that the removal efficiency of phenanthrene was higher in  
352 column B than in column A over 34 days. The phenanthrene concentration in columns  
353 A (0.30  $\mu\text{mol/L}$ ) and B (0.06  $\mu\text{mol/L}$ ) reached a peak value on day 20. Then, the  
354 phenanthrene concentrations in columns A and B both decreased to levels near 0.01  
355  $\mu\text{mol/L}$ , and showed no significant change in the remaining duration of the  
356 experiment. The simulated results showed that the change in phenanthrene  
357 concentrations in the columns was generally in good agreement with the experimental  
358 results. Figs. 3a-c shows the modelling results for the change in phenanthrene  
359 concentration in the effluent of columns A and B when the simulated initial  
360 concentration of phenanthrene is 0.9, 1.5, 2, and 2.5 mg/L, respectively. With the  
361 increase of phenanthrene concentration in the initial solution, the peak phenanthrene

362 concentration in the effluent of columns A and B was also larger (Figs. 3a-b). The  
363 removal efficiency of phenanthrene was also higher in column B than in column A in  
364 the initial stage (Fig. 3c). The peak of the change in phenanthrene concentration was  
365 observed in modelling results but was not appeared in the experimental results. The  
366 phenanthrene adsorption experiments showed that the maximum adsorption capacities  
367 of materials A and B for phenanthrene were 0.013 and 0.035 mg/g, respectively (Liu  
368 et al. 2019). Columns A and B contained 250.5 and 238.5 g of material, respectively.  
369 Therefore, it could be calculated that the maximum amounts of phenanthrene  
370 adsorbed by columns A and B were 3.26 and 8.35 mg, respectively. A total of 58.3 mg  
371 of phenanthrene passed through the column over the 450 days of operation, which  
372 suggested that there was significant degradation of phenanthrene within the column.  
373 Therefore, the observation for the change of phenanthrene concentrations in the  
374 modelling results may be explained by the removal of phenanthrene in columns A and  
375 B being mainly dependent on adsorption at the beginning, thereby the value displayed  
376 a gradually increasing trend with time to adsorption equilibrium. In the following  
377 section, the results showed that the phenanthrene concentration in columns A and B  
378 began to drop with the increase of biomass, and was kept at a very low value in the  
379 remaining experimental period. This indicated that adsorption potentially played an  
380 important role in a short term (e.g. 20 days), whereas, biodegradation controlled  
381 longer-term removal processes.

382

#### 383 **3.1.4. Biomass growth**

384 The simulated and experimental results for the change of biomass in SP1-SP4 of  
385 columns A and B are shown in Figs. 4a-d. The trend of biomass of columns A and B  
386 obtained from the experimental results increased from SP1 to SP2 and decreased from  
387 SP2 to SP4 along the flow path in the column. This phenomenon could be explained  
388 that the sufficient DO and carbon source supported the rapid growth of microbes from  
389 SP1 to SP2, but the gradually increased pH in the columns inhibited the microbial  
390 growth from SP2 to SP4. The modelling results for the biomass of SP1-SP4 of the  
391 columns had a similar trend as the experimental results, which also increased with  
392 distance from the influent end of the column and then subsequently dropped (Figs.  
393 4a-b). Moreover, the modelling and experimental results both showed that the  
394 biomass in samples from ports SP1-SP3 of columns A ( $p < 0.01$ ) and B ( $p < 0.01$ )  
395 were respectively higher than those in the initial materials A and B. In addition, the  
396 biomass in column B was higher ( $p < 0.05$ ) than in column A (Figs. 4c-d), which  
397 meant that material B was more suitable for microbial growth than material A. These  
398 data suggested that the modelling results were generally in agreement with the  
399 experimental results. The microbial yield coefficient ( $Y_x$ ) of column B was also higher  
400 than column A. Therefore, column B might have a greater potential for supporting  
401 microbial growth.

402

#### 403 **3.2. Limitations and challenges of modelling the column experiment**

404 Whether the column experiment could be simulated sufficiently well by numerical  
405 methods depends on: (1) the experimental data obtained; (2) the modelling tools and  
406 methods; (3) the theoretical analysis; (4) the relationship between the experiment and  
407 modelling. One of the challenges of simulating the column experiment was that it was  
408 difficult to exactly model the slow-release of organic carbon from materials A and B  
409 due to the lack of related experimental data. In order to achieve a reasonably accurate  
410 agreement between experimental data and simulation results for TOC, we simulated  
411 the consumption of organic carbon to represent the change of organic carbon in  
412 columns A and B.

413

#### 414 **4. Conclusions**

415 The removal process of phenanthrene from groundwater using PRB technology  
416 including adsorption and biodegradation was simulated with a reactive transport  
417 model based on the PHREEQC code and the simulation results were generally in  
418 agreement with the experimental results. The results of numerical simulations showed  
419 a deeper understanding of the removal process for phenanthrene in columns A and B,  
420 and predicted that B had a higher removal efficiency than A before 34 days. The  
421 removal efficiency of phenanthrene in both A and B was close to 100% in the PRB  
422 system. Based on the conceptual model and simulation results, adsorption played an  
423 important role in a short term, however, biodegradation controlled longer-term  
424 phenanthrene removal processes. Additionally, the content of the biomass in column

425 B was higher ( $p < 0.05$ ) than in column A, which indicated that material B was more  
426 suitable for microbial growth than material A. Therefore, material B might have a  
427 greater potential for effective biodegradation than material A in the longer term.

428

#### 429 **Data Availability Statement**

430 Some or all data, models, or code that support the findings of this study are available  
431 from the corresponding author upon reasonable request.

432

#### 433 **Acknowledgments**

434 We gratefully acknowledge the National Key R&D Program of China  
435 (2018YFD0800201 and 2018YFC1800806), the Environmental Protection  
436 Department of Jiangsu Province of China (Grant No. 2017001-1), and the Jiangsu  
437 Provincial Water Resources Department (Grant No. 2019064) for their financial  
438 support. Cuicui Liu was supported by the China Scholarship Council (No.  
439 201806190133).

440

#### 441 **References**

442 Acharya, K., Werner, D., Dolfing, J., Meynet, P., Tabraiz, S., Baluja, M.Q.,  
443 Petropoulos, E., Mrozik, W., Davenport, R.J. 2019. "The experimental determination  
444 of reliable biodegradation rates for mono-aromatics towards evaluating QSBR  
445 models." *Water Res.* 160: 278-287.

446 Ai, S.B. 2007. "Traveling waves in a bioremediation model." *SIAM J. Appl. Math.* 68  
447 (3): 680-693.

448 Akobi, C., Hafez, H., Nakhla, G. 2017. "Impact of furfural on biological hydrogen  
449 production kinetics from synthetic lignocellulosic hydrolysate using mesophilic and  
450 thermophilic mixed cultures." *Int. J. Hydrog. Energy* 42 (17): 12159-12172.

451 Balakrishnan, A., kameswari Kanchinadham, S.B., Kalyanaraman, C. 2019.  
452 "Evaluation and kinetic study on enzyme supplementation to biological treatment of  
453 vegetable tanning process wastewater." *Int. J. Environ. Sci. Technol.* 16 (10):  
454 5945-5954.

455 Bartzas, G., Komnitsas, K. 2010. "Solid phase studies and geochemical modelling of  
456 low-cost permeable reactive barriers." *J. Hazard. Mater.* 183 (1-3): 301-308.

457 Basu, A., Johnson, T.M. 2012. "Determination of hexavalent chromium reduction  
458 using Cr stable isotopes: isotopic fractionation factors for permeable reactive barrier  
459 materials." *Environ. Sci. Technol.* 46 (10): 5353-5360.

460 Berge, N.D., Reinhart, D.R., Dietz, J.D., Townsend, T. 2007. "The impact of  
461 temperature and gas-phase oxygen on kinetics of in situ ammonia removal in  
462 bioreactor landfill leachate." *Water Res.* 41 (9): 1907-1914.

463 Boluda-Botella, N., Valdes-Abellan, J., Pedraza, R. 2014. "Applying reactive models  
464 to column experiments to assess the hydrogeochemistry of seawater intrusion:  
465 optimising ACUAINTRUSION and selecting cation exchange coefficients with  
466 PHREEQC." *J. Hydrol.* 510: 59-69.



467 Broholm, K., Hansen, A.B., Jorgensen, P.R., Arvin, E., Hansen, M. 1999. "Transport  
468 and biodegradation of creosote compounds in a large, intact, fractured clayey till  
469 column." *J. Contam. Hydrol.* 39 (3-4): 331-348.

470 Caporaso, J.G., Lauber, C.L., Walters, W.A., Berg-Lyons, D., Huntley, J., Fierer, N.,  
471 Owens, S.M., Betley, J., Fraser, L., Bauer, M., Gormley, N., Gilbert, J.A., Smith, G.,  
472 Knight, R. 2012. "Ultra-high-throughput microbial community analysis on the  
473 Illumina HiSeq and MiSeq platforms." *Isme J.* 6 (8): 1621-1624.

474 Caporaso, J.G., Lauber, C.L., Walters, W.A., Berg-Lyons, D., Lozupone, C.A.,  
475 Turnbaugh, P.J., Fierer, N., Knight, R. 2011. "Global patterns of 16S rRNA diversity  
476 at a depth of millions of sequences per sample." *P. Natl. Acad. Sci. USA* 108:  
477 4516-4522.

478 Carboneras, B., Villaseñor, J., Fernandez-Morales, F.J. 2017. "Modelling aerobic  
479 biodegradation of atrazine and 2, 4-dichlorophenoxy acetic acid by mixed-cultures."  
480 *Bioresour. Technol.* 243: 1044-1050.

481 Carvajal, A., Akmirza, I., Navia, D., Pérez, R., Muñoz, R., Lebrero, R. 2018. "Anoxic  
482 denitrification of BTEX: biodegradation kinetics and pollutant interactions." *J.*  
483 *Environ. Manage.* 214: 125-136.

484 Chen, T.Y., Kao, C.M., Chiou, H.Y., Yu, Y.T., Sung, W.P. 2012. "Application of  
485 oxygen-releasing material to enhance in situ aerobic bioremediation." *Adv. Mater.*  
486 *Res.*

487 Chen, Z.Q., McTernan, W.F. 1992. "Multi-substrate, multi-option groundwater

488 transport model." *J. Contam. Hydrol.* 11 (3-4): 215-244.

489 Cobas, M., Ferreira, L., Sanromán, M.A., Pazos, M. 2014. "Assessment of sepiolite as  
490 a low-cost adsorbent for phenanthrene and pyrene removal: kinetic and equilibrium  
491 studies." *Ecol. Eng.* 70: 287-294.

492 Cogle, A.L., Saffigna, P.G., Strong, W.M. 1989. "Carbon transformations during  
493 wheat straw decomposition." *Soil Biol. Biochem.* 21 (3): 367-372.

494 Ebihara, T., Bishop, P.L. 2002. "Influence of supplemental acetate on bioremediation  
495 for dissolved polycyclic aromatic hydrocarbons." *J. Environ. Eng. (New York)* 128 (6):  
496 505-513.

497 Ferreira, L., Cobas, M., Tavares, T., Sanromán, M.A., Pazos, M. 2013. "Assessment  
498 of *Arthrobacter viscosus* as reactive medium for forming permeable reactive  
499 biobarrier applied to PAHs remediation." *Environ. Sci. Pollut. Res.* 20 (10):  
500 7348-7354.

501 Folch, A., Vilaplana, M., Amado, L., Vicent, T., Caminal, G. 2013. "Fungal permeable  
502 reactive barrier to remediate groundwater in an artificial aquifer." *J. Hazard. Mater.*  
503 262: 554-560.

504 Gandhi, S., Oh, B.T., Schnoor, J.L., Alvarez, P.J.J. 2002. "Degradation of TCE, Cr(VI),  
505 sulfate, and nitrate mixtures by granular iron in flow-through columns under different  
506 microbial conditions." *Water Res.* 36 (8): 1973-1982.

507 Geng, X.L., Boufadel, M.C., Wrenn, B. 2013. "Mathematical modeling of the  
508 biodegradation of residual hydrocarbon in a variably-saturated sand column."

509 *Biodegradation* 24 (2): 153-163.

510 Hannam, M.L., Bamber, S.D., Galloway, T.S., Moody, A.J., Jones, M.B. 2010.

511 "Effects of the model PAH phenanthrene on immune function and oxidative stress in

512 the haemolymph of the temperate scallop *Pecten maximus*." *Chemosphere* 78 (7):

513 779-784.

514 Haritash, A.K., Kaushik, C.P. 2009. "Biodegradation aspects of Polycyclic Aromatic

515 Hydrocarbons (PAHs): A review." *J. Hazard. Mater.* 169 (1-3): 1-15.

516 Kohfahl, C., Pekdeger, A. 2006. "Rising groundwater tables in partly oxidized pyrite

517 bearing dump-sediments: Column study and modelling approach." *J. Hydrol.* 331

518 (3-4): 703-718.

519 Krishnan, J., Kishore, A.A., Suresh, A., Madhumeetha, B., Prakash, D.G. 2017.

520 "Effect of pH, inoculum dose and initial dye concentration on the removal of azo dye

521 mixture under aerobic conditions." *Int. Biodeterior. Biodegradation* 119: 16-27.

522 Lee, Y.-Y., Fan, C. 2020. "Mechanistic exploration of the catalytic modification by

523 co-dissolved organic molecules for micropollutant degradation during fenton

524 process." *Chemosphere* 258: 127338.

525 Lin, C.W., Wu, C.H., Guo, P.Y., Chang, S.H. 2017. "Innovative encapsulated

526 oxygen-releasing beads for bioremediation of BTEX at high concentration in

527 groundwater." *J. Environ. Manage.* 204: 12-16.

528 Liu, C.C., Chen, X.H., Mack, E.E., Wang, S., Du, W.C., Yin, Y., Banwart, S.A., Guo,

529 H.Y. 2019. "Evaluating a novel permeable reactive bio-barrier to remediate

530 PAH-contaminated groundwater." *J. Hazard. Mater.* 368: 444-451.

531 Lokshina, L.Y., Vavilin, V.A., Kettunen, R.H., Rintala, J.A., Holliger, C.,  
532 Nozhevnikova, A.N. 2001. "Evaluation of kinetic coefficients using integrated Monod  
533 and Haldane models for low-temperature acetoclastic methanogenesis." *Water Res.* 35  
534 (12): 2913-2922.

535 McClure, P.D., Sleep, B.E. 1996. "Simulation of bioventing for soil and ground-water  
536 remediation." *J. Environ. Eng.* 122 (11): 1003-1012.

537 Mohanty, S.K., Valenca, R., Berger, A.W., Yu, I.K.M., Xiong, X.N., Saunders, T.M.,  
538 Tsang, D.C.W. 2018. "Plenty of room for carbon on the ground: Potential applications  
539 of biochar for stormwater treatment." *Sci. Total Environ.* 625: 1644-1658.

540 Moscoso, F., Deive, F.J., Longo, M.A., Sanroman, M.A. 2012. "Technoeconomic  
541 assessment of phenanthrene degradation by *Pseudomonas stutzeri* CECT 930 in a  
542 batch bioreactor." *Bioresour. Technol.* 104: 81-89.

543 Obiri-Nyarko, F., Kwiatkowska-Malina, J., Malina, G., Kasela, T. 2015.  
544 "Geochemical modelling for predicting the long-term performance of zeolite-PRB to  
545 treat lead contaminated groundwater." *J. Contam. Hydrol.* 177: 76-84.

546 Pantić, K., Bajić, Z.J., Veličković, Z.S., Nešić, J.Z., Đolić, M.B., Tomić, N.Z.,  
547 Marinković, A.D. 2019. "Arsenic removal by copper-impregnated natural mineral tufa  
548 part II: a kinetics and column adsorption study." *Environ. Sci. Pollut. Res.:* 1-19.

549 Safdari, M.S., Kariminia, H.R., Rahmati, M., Fazlollahi, F., Polasko, A., Mahendra, S.,  
550 Wilding, W.V., Fletcher, T.H. 2018. "Development of bioreactors for comparative

551 study of natural attenuation, biostimulation, and bioaugmentation of  
552 petroleum-hydrocarbon contaminated soil." *J. Hazard. Mater.* 342: 270-278.

553 Sponza, D.T., Gok, O. 2011. "Effects of sludge retention time and biosurfactant on the  
554 treatment of polyaromatic hydrocarbon (PAH) in a petrochemical industry  
555 wastewater." *Water Sci. Technol.* 64 (11): 2282-2292.

556 Tebes-Stevens, C., Valocchi, A.J., VanBriesen, J.M., Rittmann, B.E. 1998.  
557 "Multicomponent transport with coupled geochemical and microbiological reactions:  
558 model description and example simulations." *J. Hydrol.* 209 (1-4): 8-26.

559 Verce, M.F., Ulrich, R.L., Freedman, D.L. 2000. "Characterization of an isolate that  
560 uses vinyl chloride as a growth substrate under aerobic conditions." *Appl. Environ.*  
561 *Microbiol.* 66 (8): 3535-3542.

562 Waigi, M.G., Kang, F.X., Goikavi, C., Ling, W.T., Gao, Y.Z. 2015. "Phenanthrene  
563 biodegradation by sphingomonads and its application in the contaminated soils and  
564 sediments: A review." *Int. Biodeterior. Biodegradation* 104: 333-349.

565 Wang, P., Zhang, Y.M., Jin, J., Wang, T.H., Wang, J., Jiang, B.Y. 2020. "A  
566 high-efficiency phenanthrene-degrading *Diaphorobacter* sp. isolated from  
567 PAH-contaminated river sediment." *Sci. Total Environ.*: 140455.

568 Wu, C.F., Shimaoka, T., Nakayama, H., Komiya, T. 2015. "Kinetics of nitrous oxide  
569 production by denitrification in municipal solid waste." *Chemosphere* 125: 64-69.

570 Yeh, C.H., Lin, C.W., Wu, C.H. 2010. "A permeable reactive barrier for the  
571 bioremediation of BTEX-contaminated groundwater: Microbial community

572 distribution and removal efficiencies." *J. Hazard. Mater.* 178 (1-3): 74-80.

573 Zhang, J.M., Jiang, X.C., Feng, C.P., Hao, H.L. 2017. "Wheat straw, sawdust, and  
574 biodegradable plastics as potential carbon sources for synthetic nitrate-polluted  
575 groundwater column denitrification." *Desalination Water Treat.* 77: 321-330.

576 Zhang, M., Feng, Y.D., Zhang, D.Y., Dong, L.F., Pan, X.L. 2019.  
577 "Ozone-encapsulated colloidal gas aphyrons for in situ and targeting remediation of  
578 phenanthrene-contaminated sediment-aquifer." *Water Res.* 160: 29-38.

579 Zhang, W.C., Zhu, J.Q., Zhou, X.G., Li, F.H. 2018. "Effects of shallow groundwater  
580 table and fertilization level on soil physico-chemical properties, enzyme activities,  
581 and winter wheat yield." *Agr. Water Manage.* 208: 307-317.

582

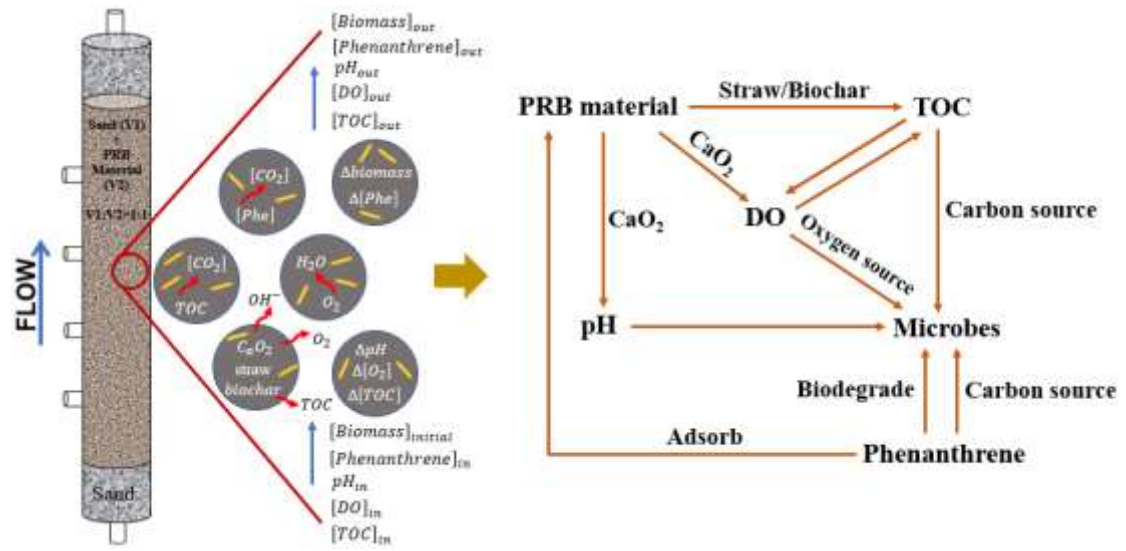


**Fig. 1.** A conceptual model for modelling the process of the column experiment.

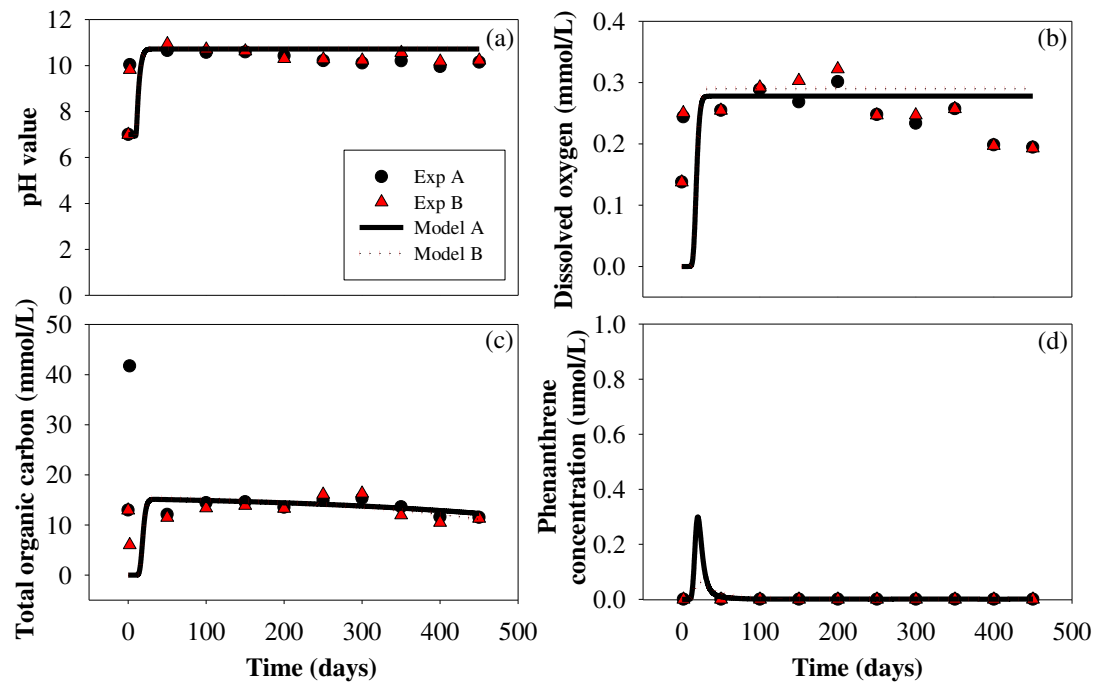


**Fig. 2.** Simulated (lines) and experimental (symbols) results for variations in (a) pH value, (b) dissolved oxygen, (c) total organic carbon, and (d) phenanthrene concentration in the effluents of the columns A and B.



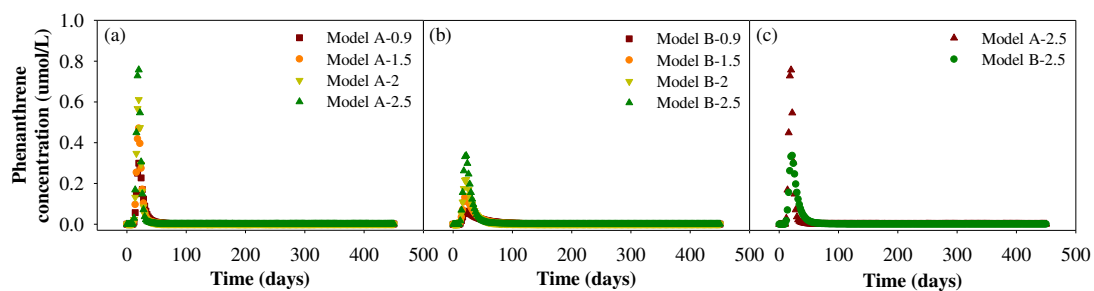


**Fig. 3.** Modelling results for the change of phenanthrene concentration in the effluents of (a) column A and (b) column B when the initial concentration of phenanthrene was 0.9, 1.5, 2, and 2.5 mg/L, respectively. (c) The comparison of modelling results for phenanthrene concentration in the effluents of columns A and B (with an initial phenanthrene concentration of 2.5 mg/L).

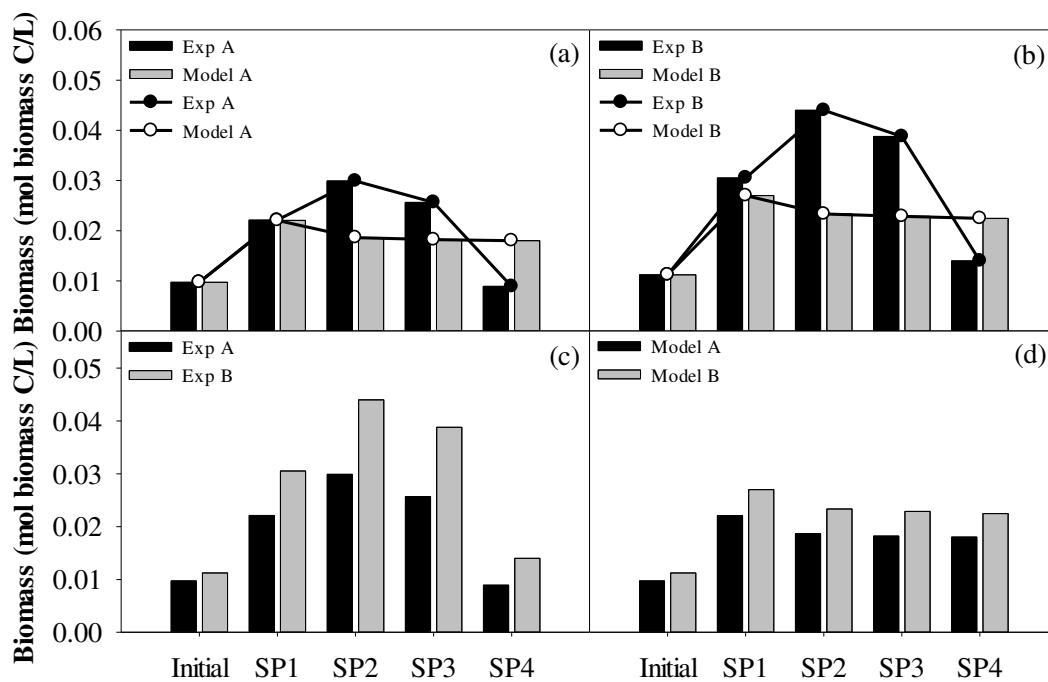


**Fig. 4.** The comparison of simulated and experimental results of the biomass from the initial materials and samples collected from ports SP1-4 of columns (a) A and (b) B. The (c) experimental and (d) simulated results for the biomass in columns A and B.

**Table 1.** General characteristics of raw materials used in the PRB material

Raw material	Fractionation	Particle size range
Wood brick	granule	2-4 mm
Wheat straw	powder	550-700 $\mu\text{m}$
Coconut shell biochar	powder	150-180 $\mu\text{m}$
Calcium peroxide (70%)	powder	150-180 $\mu\text{m}$
Attapulgite	powder	150-180 $\mu\text{m}$
Diatomite	powder	180-270 $\mu\text{m}$
Cement	powder	150-180 $\mu\text{m}$
Sodium alginate	powder	150-180 $\mu\text{m}$

**Table 2.** Characteristics of columns A and B used in the simulations

Parameter	Column A	Column B
Column volume (mL)	628	628
PRB material (g)	250.5	238.5
Quartz sand (g)	663.5	677
Pore volume (mL)	148.2	151.3
Porosity (%)	23.6	24.1
Hydraulic conductivity (m d <sup>-1</sup> )	0.48	0.48
Residence time (h)	24.93	24.93

**Table 3.** The ADR equations for the local change of species concentrations in porewater or solids

Species	Phase	ADR equation
Phenanthrene	porewater	$\frac{\partial C_{phen,pw}}{\partial t} = -v \frac{\partial C_{phen,pw}}{\partial x} + D_L \frac{\partial^2 C_{phen,pw}}{\partial x^2} + R_{phen,sorp} + R_{phen,bio}$
		$R_{phen,sorp} = -k_m \left( C_{phen,pw} - \frac{C_{phen,s}}{K_d} \right)$
		$R_{phen,bio} = -\frac{\mu_{max,phen} X_{phen}}{14 Y_{X_{phen}}} \frac{C_{phen,pw}}{K_{phen} + C_{phen,pw}} \frac{C_{ox,pw}}{K_{ox} + C_{ox,pw}}$
	solid	$\frac{\partial C_{phen,s}}{\partial t} = -R_{phen,sorp} K_d$
		$R_{phen,sorp} = -k_m \left( C_{phen,pw} - \frac{C_{phen,s}}{K_d} \right)$
TOC	porewater	$\frac{\partial C_{TOC,pw}}{\partial t} = -v \frac{\partial C_{TOC,pw}}{\partial x} + D_L \frac{\partial^2 C_{TOC,pw}}{\partial x^2} + R_{TOC,bio}$
		$R_{TOC,bio} = -\frac{\mu_{max,TOC} X_{TOC}}{Y_{X_{TOC}}} \frac{C_{TOC,pw}}{K_{TOC} + C_{TOC,pw}} \frac{C_{ox,pw}}{K_{ox} + C_{ox,pw}}$
Oxygen	porewater	$\frac{\partial C_{ox,pw}}{\partial t} = -v \frac{\partial C_{ox,pw}}{\partial x} + D_L \frac{\partial^2 C_{ox,pw}}{\partial x^2} + R_{ox} + 16.5 R_{phen,bio} + R_{TOC,bio}$
		$R_{ox} = \lambda$
		$R_{phen,bio} = -\frac{\mu_{max,phen} X_{phen}}{14 Y_{X_{phen}}} \frac{C_{phen,pw}}{K_{phen} + C_{phen,pw}} \frac{C_{ox,pw}}{K_{ox} + C_{ox,pw}}$
		$R_{TOC,bio} = -\frac{\mu_{max,TOC} X_{TOC}}{Y_{X_{TOC}}} \frac{C_{TOC,pw}}{K_{TOC} + C_{TOC,pw}} \frac{C_{ox,pw}}{K_{ox} + C_{ox,pw}}$
Biomass	solid	$\frac{\partial C_{bm,s}}{\partial t} = \frac{\partial X_{phen}}{\partial t} + \frac{\partial X_{TOC}}{\partial t} = R_{bm,phen} + R_{bm,TOC}$
		$R_{bm,phen} = -14 Y_{X_{phen}} R_{phen,bio} - b X_{phen}$
		$R_{bm,TOC} = -Y_{X_{TOC}} R_{TOC,bio} - b X_{TOC}$
<p><b>Note:</b> (mol L<sup>-1</sup>) → <math>C_{phen,pw}</math>; <math>K_{phen}</math>; <math>C_{ox,pw}</math>; <math>K_{ox}</math>; <math>C_{TOC,pw}</math>; <math>K_{TOC}</math>; <math>C_{bm,s}</math>  (mol biomass C L<sup>-1</sup>) → <math>X_{phen}</math>; <math>X_{TOC}</math> (mol biomass C L<sup>-1</sup> s<sup>-1</sup>) → <math>R_{bm,phen}</math>; <math>R_{bm,TOC}</math>  (mol L<sup>-1</sup> s<sup>-1</sup>) → <math>R_{phen,sorp}</math>; <math>R_{phen,bio}</math>; <math>R_{TOC,bio}</math>; <math>R_{ox}</math>; <math>\lambda</math>  (mol biomass C/mol phenanthrene C) → <math>Y_{X_{phen}}</math> (mol biomass C/mol TOC C) → <math>Y_{X_{TOC}}</math>  (s<sup>-1</sup>) → <math>k_m</math>; <math>\mu_{max,phen}</math>; <math>\mu_{max,TOC}</math>; <math>b</math> (m<sup>2</sup> s<sup>-1</sup>) → <math>D_L</math> (s) → <math>t</math>  (m s<sup>-1</sup>) → <math>v</math> (m) → <math>x</math> (mol g<sup>-1</sup>) → <math>C_{phen,s}</math> (L g<sup>-1</sup>) → <math>K_d</math></p>		

**Table 4.** Model transport parameters

Parameter	Value	Unit
Cells	10	-
Lengths	10×0.04	m
Shifts	225	-
Time_step	172800	s
Flow_direction	Forward	-
Boundary_conditions	Flux-flux	-
Diffusion_coefficient	0.03×10 <sup>-9</sup>	m <sup>2</sup> s <sup>-1</sup>
Dispersivities	0.005	m
Correct_disp	True	-

**Table 5.** Modelling parameters for the column experiment

Parameter	Column A	Column B
Phenanthrene adsorption	$k_m = 2.63 \times 10^{-4}$ (Pantić et al. 2019); $K_d = 5.33 \times 10^{-4}$ (Tebes-Stevens et al. 1998)	$k_m = 4.5 \times 10^{-4}$ (Pantić et al. 2019); $K_d = 4.27 \times 10^{-4}$ (Tebes-Stevens et al. 1998)
Phenanthrene biodegradation	$\mu_{max,phen} = 3.33 \times 10^{-6}$ (Krishnan et al. 2017); $K_{phen} = 7.1 \times 10^{-6}$ (McClure and Sleep 1996); $Y_{X_{phen}} = 0.44$ (This value fit well with the experimental data); $K_{ox} = 6.25 \times 10^{-6}$ (Tebes-Stevens et al. 1998)	$\mu_{max,phen} = 8.22 \times 10^{-7}$ (Carboneras et al. 2017); $K_{phen} = 7.1 \times 10^{-6}$ (McClure and Sleep 1996); $Y_{X_{phen}} = 0.53$ (This value fit well with the experimental data); $K_{ox} = 6.25 \times 10^{-6}$ (Tebes-Stevens et al. 1998)
TOC consumption	$\mu_{max,TOC} = 5.1 \times 10^{-8}$ (Lokshina et al. 2001); $K_{TOC} = 7.1 \times 10^{-6}$ (McClure and Sleep 1996); $Y_{X_{TOC}} = 0.932$ (This value fit well with the experimental data); $K_{ox} = 6.25 \times 10^{-6}$ (Tebes-Stevens et al. 1998)	$\mu_{max,TOC} = 5.56 \times 10^{-8}$ (Verce et al. 2000); $K_{TOC} = 7.1 \times 10^{-6}$ (McClure and Sleep 1996); $Y_{X_{TOC}} = 0.954$ (This value fit well with the experimental data); $K_{ox} = 6.25 \times 10^{-6}$ (Tebes-Stevens et al. 1998)
Biomass	$b = 1.16 \times 10^{-8}$ (Chen and McTernan 1992)	$b = 1.16 \times 10^{-8}$ (Chen and McTernan 1992)